J. Electrochem. Sci. Eng. **12(4)** (2022) 703-719; http://dx.doi.org/10.5599/jese.1305

Open Access : : ISSN 1847-9286
www.jESE-online.org

Original scientific paper

Cerium-based conversion films developed on LiAl-layered double hydroxide coatings for corrosion protection of AA7075 aluminum alloys

Aurora Petica[1], Adrian Cristian Manea[1], Geanina Mihai[1], Ioana Nicola[2], Victoria Ceara[2] and Liana Anicai[1,✉]

[1]*Center of Surface Science and Nanotechnology, University Politehnica of Bucharest, Splaiul Independentei 313, 060042 Bucharest, Romania*
[2]*ICPE-SA, Splaiul Unirii 313, 030138, Bucharest, Romania*

Corresponding author: ✉lanicai@itcnet.ro; Tel.: +40 21 4029100; Fax: +40 21 3181001

Received: Febrzary 18, 2022; Accepted: June 18, 2022; Published: July 18, 2022

Abstract

The paper presents several experimental results regarding the influence of various procedures applied to incorporate Ce species in hydrotalcite–type chemical conversion coatings on the overall corrosion performance for AA 7075 aluminum alloy as a metallic substrate. Two routes were envisaged: (i) chemical incorporation of Ce by immersion in cerium nitrate solutions and (ii) electrochemical deposition of hydrophobic Ce - based layer involving ethanolic solutions of stearic acid and cerium nitrate. The chemical route involving immersion in cerium nitrate solutions led to the incorporation of 2.46 – 6.84 wt.% Ce in the composition of the porous conversion layer. The electrochemical process facilitated the formation of a hydrophobic cerium stearate layer on porous hydrotalcite conversion coating showing water contact angles of about 132° and a higher Ce content incorporated of 6.55 – 9.73 wt.%. The corrosion performance of the Ce-based conversion coatings is also discussed.

Keywords

Conversion coatings; chromium-free conversion coatings; aluminum alloys; corrosion behavior; hydrophobic layers

Introduction

The development of alternative surface pretreatments and pigmented coatings on Al and its alloys to eliminate the health hazards and toxicity of soluble hexavalent chromium has been pursued for many years. Especially in the aeronautical industry, the replacement or elimination of hexavalent chromium has been and still is a major challenge [1-5]. Chromate-containing conversion coatings (CCs) are among the most developed and large-scale applied to protect Al alloys with superior performance.

Whilst many approaches have been attempted to achieve acceptable alternatives, relatively few systems have demonstrated similar effectiveness as chromate-containing systems [6,7].

A variety of investigations have been performed to find suitable candidates to replace chromates. Ideally, these compounds should have a similar performance as chromates, i.e., providing corrosion protection to the substrate and serving as a reservoir of corrosion inhibitor, which has the ability to be released from the coating when damages occur and heal the defect by the formation of a protective or passivation layer. This leaching of soluble chemical species is the main corrosion-inhibiting strategy used in corrosion-inhibiting coating technology for the protection of high-strength Al alloys [8,9].

Rare earth compounds are among the most promising options for replacing chromate conversion coatings on Al [10,11]. Such compounds have been found to act as cathodic inhibitors, including Ce, Sm, La, Nd, Pr, Y, Gd and Tb. Cerium compounds are generally the most active and the corrosion resistance usually follows the sequence: Ce > Nd > Pr > Y > La. With the exception of La, the other rare earth agents are effectively ruled out of widespread commercial use due to cost considerations. However, La-containing coating not only is less active than Ce one but also shows poor adhesion as well. Thus, usually, the term „rare earth" is to be considered to mean cerium [10 and included refs.].

Cerium-based conversion coatings can be applied to Al alloys by a large range of procedures, including electrolytic deposition, spray, swabbing and immersion. Immersion processes may be either (i) unaccelerated or (ii) accelerated thermally or chemically [10,12,13 and included refs.]. Most of the investigations have been focused on immersion processes because both electrodeposition and spray deposition were found to still have several hurdles facing them before being considered for a mainstream application.

The use of rare-earth compounds as corrosion inhibitors has been proposed for the first time by Hinton and his co-workers in Australia [14,15], who involved Ce salts in protecting Al-based substrates, thus providing excellent resistance to localized corrosion. Hughes *et al.* [16] investigated the generation of Ce- and Mo- containing CC coatings on Al alloy by a multistep process. In spite of excellent corrosion performance, the proposed procedures are unsuitable for a large-scale application due to the long period required (more than 24 h). Therefore, for any practical purpose, an accelerated process should be used. Usually, the deposition of cerium oxide/hydroxide-based coatings occurs at local cathodic sites, where the pH is increased, depending on the operation parameters, which should be rigorously controlled because they influence both the formation kinetics and their final protective characteristics [10,13,17]. Application of post-coating seals is also recommendable [10,18].

The application of thinner coatings demands new strategies to extend their lifetime and improve their effectiveness. New synthesis routes and procedures have been reported in order to improve corrosion protection of Al alloys while benefitting from the characteristics Ce-based compounds may provide.

Under these circumstances, combinations of Ce-based conversion coatings with layered double hydroxides (LDHs) or various types of sol-gel films have also been reported. LDH is a hydrotalcite-like compound, which is typically composed of positively-charged mixed metal M^{II}-M^{III} hydroxide layers and interlayers occupied by anions (A^{y-}) and water molecules [19,20]. The pioneering work of Buchheit *et al.* [21] showed that a coating consisting in a hydrotalcite (HT) layer (formed by immersion in a bath containing a mixture of lithium, potassium, and sodium salts), sealed by contact with Ce solutions, exhibits self-healing behaviour probably because Ce is introduced into the HT as a soluble high-oxidation-state species. LDHs have often been employed as containers for corrosion inhibitors such as

rare earth ions to provide active corrosion protection for the metal substrates. In addition, Visser *et al.* [22,23] recently showed that Li salts are also of interest as an alternative corrosion inhibitor to protect Al alloys after earlier reports of Buchheit *et al.* [24,25] regarding the passivity of Al in alkaline lithium salt solutions. It has also been shown that the lithium-leaching coatings also suppressed localized corrosion and provided additional corrosion resistance on more corrosion-resistant aluminium alloys such as AA5083-H111 and AA6014-T4, by the formation of a protective layer in the defect area and preventing local corrosion processes despite the different intrinsic electrochemical activity of the alloys [26]. Fernandes *et al.* [27] showed that hydrotalcite (denoted HT-HTC) based coatings formed onto AA 6061 alloy involving lithium nitrate solutions showed an increased corrosion performance compared to those formed in lithium carbonate ones. Moreover, Ce incorporation in the HT-HTC layer further enhanced the metallic substrate's corrosion resistance. Recently, Zhang *et al.* [28] reported the synthesis of Ce-doped Zn-Al LDHs and their incorporation into a hybrid sol-gel protective coating for AA2024. The sol-gel coating modified with Ce-doped Zn-Al LDHs exhibited higher corrosion protection behavior compared with both unmodified and Ce-undoped LDHs containing coatings. This proved the applicability of Ce-doped LDHs in delaying coating degradation and their potential application as nanocontainers of corrosion inhibitors in self-healing coatings. Chen *et al.* [29] prepared double-doped LDH films on AA2024, using Ce(III) and vanadate species as dopants through a two-step procedure involving: (i) the in-situ growth of Ce-doped ZnAl LDH with urea hydrolysis followed by (ii) the intercalation of $V_2O_7^{4-}$ by the anion-exchange process. The performed EIS (electrochemical impedance spectroscopy) investigations involving the immersion in 0.05 M NaCl solution for 15 days showed that the double incorporation of Ce(III) and $V_2O_7^{4-}$ significantly enhances the corrosion performance, exhibiting high impedance values of $\approx 10^6$ Ω cm^2 order. However, the proposed procedure suffers from a quite long synthesis procedure (24 h for the first step followed by 2 h for the second one).

Iqbal and Fedel [30] applied Ce-doped MgAl LDHs directly on the anodized aluminum surface and on the hot-water sealed anodized aluminum specimens at 80 °C for 18 h. According to EIS investigations during immersion in 0.1 M NaCl solution for 1200 h, it was found that the addition of Ce ions facilitated improved corrosion protection, mainly when the growth of CeMgAl-LDHs has been developed on the anodized layer. To get more information on the role of trivalent cerium species present in Ce-doped MgAl LDHs, Fedel and Zampiccoli [31] developed the conversion layers directly on the 6082 aluminum alloy surface at 80 °C for preparation periods between 1 and 9 h. The analysis of the data acquired before and after 400 h of continuous immersion in the 0.1 M NaCl, suggested a corrosion inhibition mechanism based on the dissolution and re-precipitation of Ce compounds.

In order to enhance the corrosion protection of aluminum alloys and inspired by nature, the development of highly hydrophobic/superhydrophobic surfaces has also been considered an attractive strategy. In particular, the specific morphology of LDH-based conversion layers might facilitate superhydrophobic characteristics upon modification with low-surface-energy chemicals [32]. In this regard, Yang *et al.* [33] reported the preparation of Li-Al LDH coating on AA2099-T83 Al-Cu-Li alloy, followed by 1H, 1H, 2H, 2H- perfluorodecyl trimethoxysilane (PFDTMS) modification. The modified layer showed superhydrophobic properties with a water contact angle of about 155° and superior corrosion performance materialized by a corrosion current decrease of two orders of magnitude. Iqbal *et al.* [34] prepared superhydrophobic Ce-doped MgAl LDHs directly on the anodic surface of AA6082 alloy through modification by PFDTS (1H, 1H, 2H, 2H perfluorododecyl trichlorosilane) through anion exchange reaction, exhibiting high water contact angle of about 156°, improved corrosion resistance and self-cleaning properties. While some superhydrophobic surface layers on

various aluminum and aluminum alloys have been developed as an efficient barrier against corrosion, they mostly involve the use of fluorinated chemicals, which negatively affect the environment and human health. In this context, the use of fatty acids, including myristic acid (CH_3-$(CH_2)_{12}$-COOH), stearic acid (CH_3-$(CH_2)_{16}$-COOH), or decanoic acid (CH_3–$(CH2)_8$–COOH) could represent an attractive more environmentally friendly route [35]. Iqbal *et al.* [36] used 0.01 M sodium stearate solution at 50 °C for 5 h to develop the superhydrophobic structure over Ce doped MgAl LDH grown directly on an anodized AA6082 surface, which exhibited a water contact angle of ~155°. It has been shown that the obtained layers presented superior corrosion resistance characteristics in 0.1 M NaCl, also benefitting from the synergic effect of cerium inhibitors and superhydrophobic surfaces.

Quite recently, Zhang *et al.* [37,38] proposed an easier and quicker approach to fabricating superhydrophobic surfaces directly on pure Al substrate, involving a one-step electrodeposition process and ethanolic solutions of myristic acid or stearic acid and cerium nitrate under constant voltage conditions. The electrochemically prepared superhydrophobic surfaces showed greatly enhanced corrosion resistance and good lasting quality under air exposure and 3.5 wt.% NaCl immersion.

Considering all mentioned above, the present paper intends to explore the influence of various procedures applied to incorporate Ce species in hydrotalcite–type chemical conversion coatings, on the overall corrosion performance, for AA 7075 aluminum alloy as a metallic substrate. Two routes were envisaged: (i) chemical immersion in cerium nitrate solutions and (ii) electrochemical deposition of hydrophobic Ce-based layer involving ethanolic solutions of stearic acid and cerium nitrate. In this context, it is worth mentioning that, to the best of our knowledge, no hydrophobic coating was reported on HT layers or AA 7075 aluminum alloy involving electrolytes based on Ce salts and stearic acid.

Experimental

In order to perform experiments, unpolished specimens of AA 7075 alloy (chemical composition shown in Table 1) have been cut in 35×70×10 mm coupons and used as metallic substrate.

Table 1. *Chemical composition of AA 7075*

Content, wt.%									
Si	Fe	Cu	Mn	Mg	Cr	Zn	Ti	Other	Al
Max. 0.40	Max. 0.50	1.2-2.0	Max. 0.30	2.1-2.9	0.18-0.28	5.1-6.1	Max. 0.2	Max. 0.15	rest

Before any process, the specimens have been firstly degreased in acetone for 30–60 s to remove surface contaminations. Then, a chemical alkaline degreasing step was applied using an aqueous solution of 30–50 g/L $Na_2CO_3{\cdot}10H_2O$ + 30–50 g/L $Na_3PO_4{\cdot}12H_2O$ + 5 g/L NaOH, for 5 min. at 60–80 °C, followed by a chemical desmutting in HNO_3 1:1 (vol.) solution containing 0.37 % $CeCl_3$ [39] for 30–60 s at room temperature, water rinsing and drying. The specimens have been rinsed in deionized water between each step, too.

The hydrotalcite type conversion coatings (denoted HT) have been developed by immersion at a constant temperature of 90±5 °C for 20 min. in solutions containing a mixture of lithium and potassium salts, whose detailed composition is presented in Table 2. The HT-coated surfaces were rinsed with distilled water and then subjected to the Ce species incorporation step, either (i) by immersion in 0.05 M $Ce(NO_3)_3{\cdot}6H_2O$ solution for 20 min. (specimens denoted HT-Ce) or (ii) by electrochemical deposition of hydrophobic Ce-based layer in ethanolic solutions of 0.1 M $Ce(NO_3)_3{\cdot}6H_2O$ + 0.1 M stearic acid at a constant voltage (U_{dc}) of 20 V for 20 min., at room temperature (specimens

denoted HT-Ce-S). In this case, a two-electrode cell configuration has been used, where platinized titanium plates acted as anode. After preparation, the specimens were rinsed with ethanol and dried using an air blower.

Table 2. *Chemical composition and applied operating parameters during conversion coatings preparation*

Conversion type	Solution composition	Operating parameters
HT	6.9 g L^{-1} $LiNO_3$; 28.3 g L^{-1} KNO_3 2.4 g L^{-1} LiOH; pH 12 - 12.5	t = 20 min T = 90 ± 5 °C
HT-Ce	0.05 M $Ce(NO_3)_3 \cdot 6H_2O$	t = 20 min T = 23 ± 2 °C
HT-Ce-S	0.1 M $Ce(NO_3)_3 \cdot 6H_2O$ 0.1 M stearic acid in ethanol	$U_{dc(const)}$ = 20 V t = 20 min; T 23 ± 2 °C

Scanning electron microscopy (SEM) (Hitachi SU 8230, Hitachi High-Tech Corporation, Tokyo, Japan) and Energy dispersive X-ray spectroscopy (EDX) (Oxford Instruments, Oxford, UK) were used to analyze the surface morphology and the composition of the prepared conversion films. The investigation of the phase composition and structure of the prepared films was performed by X-ray diffractometry (XRD) (High Resolution SmartLab X-ray diffractometer Rigaku, Tokyo, Japan 9 kW, with rotating anode) using CuK_α radiation (λ = 0.15406 nm) at room temperature, in the 2θ range of 5–90 degree. To get information about the surface composition, the Fourier transform infrared (FTIR) spectrometry (Spectrum Two FT-IR instrument equipped with Universal Diamond/KRS-5 ATR component, Perkin Elmer, USA) was used and the spectra were collected from 4000 to 450 cm^{-1}.

The surface wettability characteristics of the investigated specimens have been determined by measurements of the contact angles (CAs) using a CAM 100 compact angle meter at room temperature (24±2 °C). An average value of at least five measurements performed on different areas of the specimens was considered. The hydrophilic (θ< 90°) or hydrophobic (θ> 90°) character of the prepared surfaces has been assessed using deionized water as liquid.

The assessment of corrosion behavior of the HT-Ce and HT-Ce-S conversion coatings has been performed involving accelerated laboratory tests consisting of continuous immersion in aerated 0.5 M NaCl aqueous solution at 25 °C for 360 h, with intermediary visual examinations. Minimum 3 pieces of each conversion coating type (70×35 mm) were subjected to an immersion test. Potentiodynamic polarization curves at a sweeping rate of 1 mV s^{-1} and electrochemical impedance spectra (EIS) at open-circuit potential using 0.5 M NaCl solution were recorded against Ag/AgCl reference electrode and using a Pt counter electrode. For both electrochemical investigations, the geometrical surface of the working electrode was 0.196 cm^2. EIS spectra, recorded with 10 mV a.c. voltage within 100 kHz to 100 mHz frequency range, have been processed using ZView 2.4 software from Scribner Association Inc., Derek Johnson. All electrochemical investigations have been performed using a PARSTAT 4000 potentiostat controlled with VersaStudio software.

Results and discussion

In order to develop hydrotalcite type conversion coatings (HT), AA 7075 specimens have been immersed in conversion solution for 30 min. and the open circuit potential (U_{oc}) during the time has been monitored to evidentiate the different stages of the formation as illustrated in Figure 1 (black line).

A sudden shift of the U_{oc} occurs during the first 15 s, up to -1.04 V, followed by a further displacement in the cathodic direction up to -1.11 V for about 10 min. of exposure. This is related to

the metal dissolution in the strong alkaline solution, associated with H_2 evolution from the surface. Then, Uoc started to increase as the conversion film forms, up to a quite stable value, assigned to thickening of the coating and gas evolution ceased. This gradual increase suggests a slow but continuous formation of the layer on the alloy surface. The general shape of U_{oc} recording is relatively similar to those reported in [23,40] for AA2024-T3 and pure Al substrates.

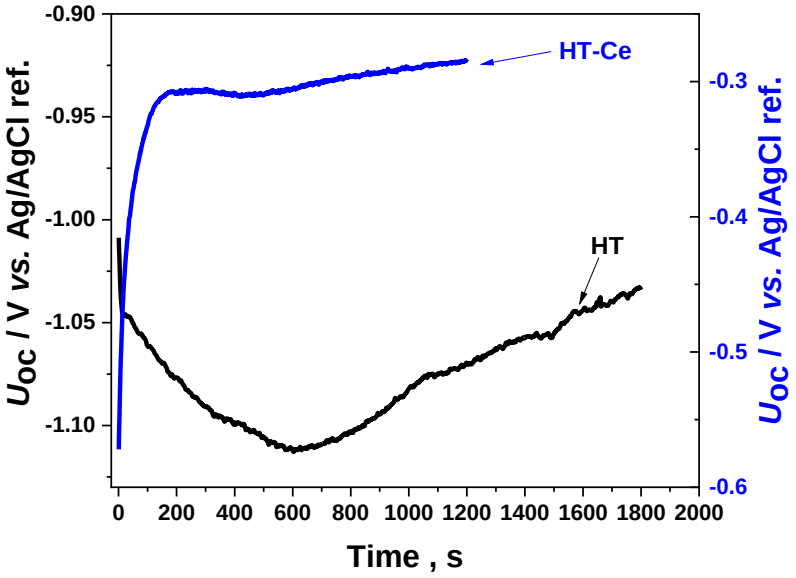

Figure 1. *Evolution of open circuit potential vs. conversion time for HT (black line) and HT-Ce (blue line) during coatings formation*

During the next Ce species incorporation step (see Figure 1 blue line), a shift of U_{oc} towards more positive values in time is noticed, assigned to the formation of a second protective layer. According to [41-43 and included references], the development of the cerium-based film on aluminum and its alloys using solutions of simple cerium salts with no presence of an oxidizing agent could occur through the participation of the dissolved oxygen in the solution. Therefore, the reduction of oxygen occurs (Eq. 1), leading to OH^- ions formation [41,43]:

$$O_2 + 2\ H_2O + 4\ e^- \rightarrow 4\ OH^- \quad (1)$$

Further, the reaction of Ce (III) species with hydroxide ions could lead to the formation of protective cerium oxide (Eq. 2) that covers the surface, also facilitated by the alkaline pH of HT coating [43]:

$$2\ Ce^{3+} + 4\ OH^- + O_2 + 2\ e^- \rightarrow 2\ CeO_2 + 2\ H_2O \quad (2)$$

SEM micrographs of the developed HT-Ce coating onto AA 7075 alloy are presented in Figure 2, at various magnifications.

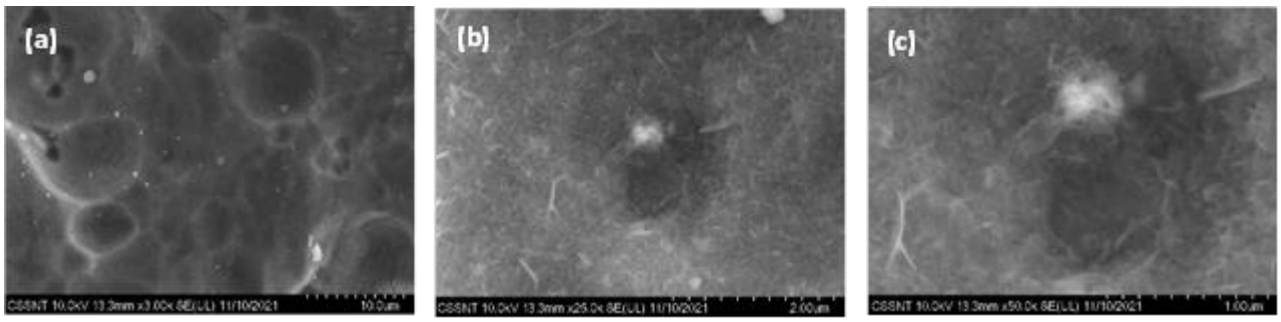

Figure 2. *SEM micrographs at different magnifications in the case of HT-Ce layer developed onto AA 7075 alloy:(a) 3000×; (b) 25000× and (c) 50000×*

A porous morphology could be noticed, entirely covering the metallic surface. At higher magnification (Figure 2b and 2c), a nest-like structure is revealed, composed of curved blade-like formations of about 10–20 nm in width and a length of 200-300 nm. Besides the presence of aluminum, oxygen, as well as of Mg, and Cu as alloying elements, EDX analysis evidenced the presence of 2.46 –6.84 wt.% Ce in the composition of HT-Ce layer.

Figure 3 presents an example of the recorded SEM micrographs at various magnifications for the HT-Ce-S coatings obtained after the electrochemical step in cerium-stearic acid ethanolic solution, applying a constant voltage of 20 V for 20 min.

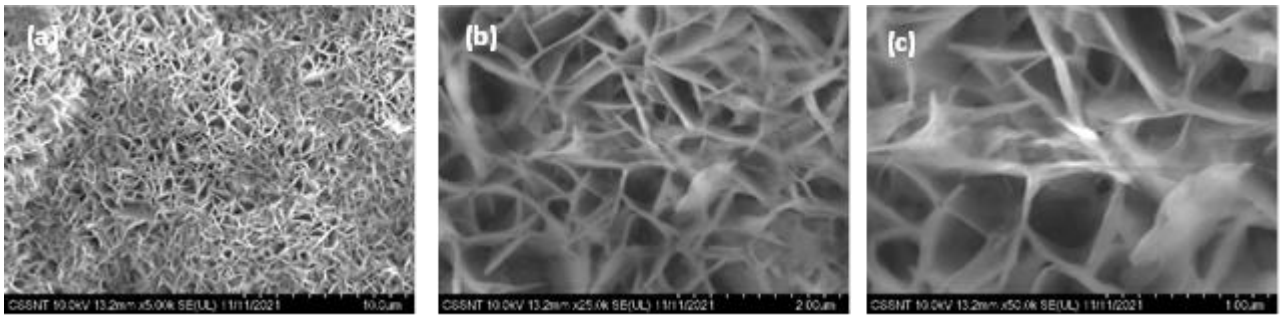

Figure 3*. SEM micrographs at different magnifications in the case of HT-Ce-S layer developed onto AA 7075 alloy: (a) 5000×; (b) 25000× and (c) 50000×*

As shown in Figure 3, a better profiled curved platelet structure developed perpendicular to the substrate is observed, also exhibiting a certain level of disorder. Traditionally, electrochemical deposition could be seen as a process occurring at the atomic/molecular level so that the formed layer entirely takes the three-dimensional shape of the substrate with very high accuracy [44].

Therefore, the applied electrochemical step on the already formed HT coating led to the formation of a quite similar morphology (not shown here), however, with much more well-defined features.

According to EDX measurements, the Ce content within the HT-Ce-S layer was higher as compared to HT-Ce ones, in the range 6.55–9.73 wt.%, suggesting an enhanced cerium ions insertion after the electrodeposition process. In addition, the presence of carbon, aluminum, oxygen, as well as of Mg and Cu as alloying elements has also been identified. The C/Ce atomic ratio calculated from EDX analysis was found to be between 49.5 (C/Ce = 42.56:0.86) and 52.77 (C/Ce = 27.44:0.52), which is relatively close to the theoretical value in cerium stearate, Ce $(CH_3(CH_2)_{16}COO)_3$, *i.e.,* C/Ce = 54:1.

In the employed cerium nitrate solution, Ce^{3+} ions resulted from dissociated cerium nitrate hexahydrate, moving toward the cathode on applying the constant voltage. Near the cathode, Ce^{3+} ions react with stearate ions available as a result of the dissociation reaction of stearic acid, forming cerium stearate over the porous HT surface. The reduction of hydrogen ions at the cathode surface also occurs, leading to the formation and release of gaseous hydrogen, evidenced by the presence of bubbles. Consequently, the following reactions can be formulated:

$$CH_3(CH_2)_{16}COOH \leftrightarrow CH_3(CH_2)_{16}COO^- + H^+ \quad (3)$$

$$Ce^{3+} + 3\ CH_3(CH_2)_{16}COO^- \rightarrow Ce\ (CH_3(CH_2)_{16}COO^-)_3 \quad (4)$$

$$2\ H^+ + 2\ e^- \rightarrow H_2\uparrow \quad (5)$$

Figure 4 presents the XRD patterns of HT-Ce and HT-Ce-S films developed on AA 7075 alloy. The characteristic peaks located at 38.4, 44.7, 64.9 and 78° were assigned to the Al phase of AA 7075 alloy [45]. In addition, peaks occurring at around 10 and 20° suggest the formation of LDH

intercalated with NO_3^- [28,29,45-48]. However, slight shifts of the diffraction peaks ascribed to (003) and (006) reflections suggest the cerium species intercalated in the hydrotalcite structure.

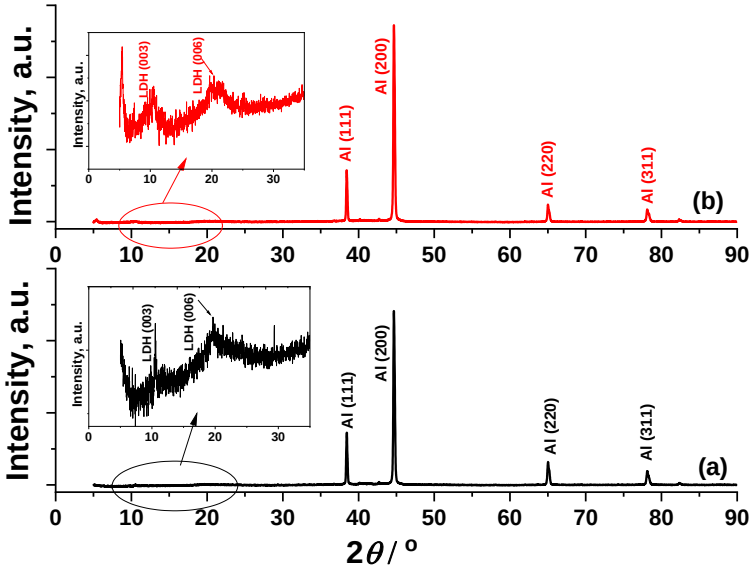

Figure 4. *XRD patterns of: (a) HT-Ce and (b) HT-Ce-S films developed on 7075 Al alloy*

The peak related to (003) reflection is displaced from 11.64 to 10.51°, while the peak corresponding to (006) reflection is repositioned from 23.40 to 19.76°. Based on the Bragg's equation, the d-spacing value of the (003) reflection increased from 0.760 nm to 0.841 nm and the d-spacing value of the (006) reflection enlarged from 0.3801 nm to 0.4489 nm. The low intensity of (003) and (006) reflections suggests a decline of the LDH crystallinity. As similar XRD patterns were recorded both for HT-Ce and HT-Ce-S films, it could be considered that the type of procedure, i.e., either chemical or electrochemical, does not produce a significant change in the layer's structure.

FT-IR spectra of HT-Ce and HT-Ce-S films are presented in Figure 5.

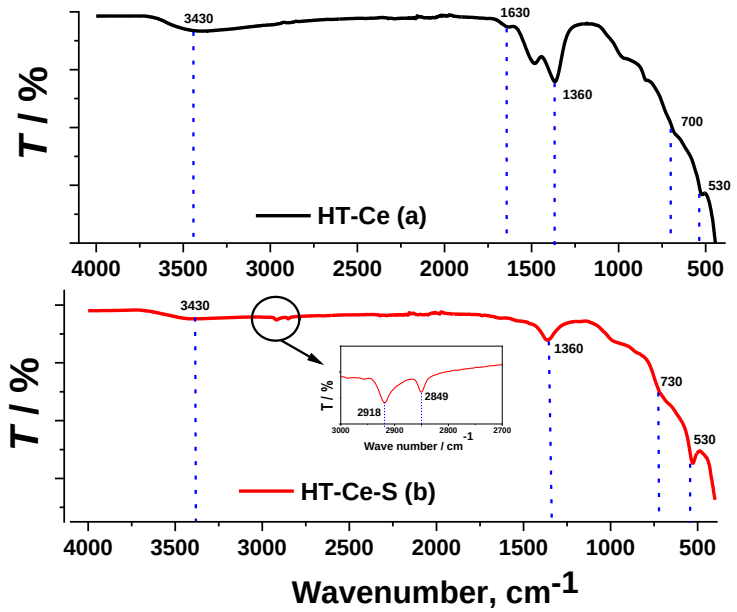

Figure 5*. FTIR/ATR spectra related to (a) HT-Ce and (b) HT-Ce-S layers onto AA 7075 alloy*

The spectrum of the HT-Ce layer (see Figure 5a) exhibits a broad shoulder centered at about 3430 cm^{-1}, assigned to O-H stretching vibration of the LDHs layer as well as to interlayer water molecules

bonded to LiAl-OH groups [48,49]. The low-resolution adsorption peak is located at about 1630 cm^{-1} was ascribed to the bending mode of water molecules, indicating a small amount of interlayer water in the LiAl-based LDH [50]. The adsorption band present at about 1360 cm^{-1} corresponds to the NO_3^- anions stretching vibration. The peaks located between 720 cm^{-1} and 530 cm^{-1} can be assigned to M=O and M-OH (M = Al, Li) lattice vibrations in LDH layers [48]. After electrochemical modification involving stearic acid-cerium nitrate ethanolic solutions, two additional peaks located at 2918 cm^{-1} and 2849 cm^{-1} are evidenced (see Figure 5b), related to stearic acid and attributed to (-CH-) asymmetric and symmetric stretch vibration, respectively [38,51]. The above-mentioned results associated with the presence of Ce and of the determined C/Ce atomic ratio, as evidenced from EDX analysis, suggest the formation of a cerium stearate (Ce $[(CH_3(CH_2)_{16}COO]_3$) on the HT formed layer on AA 7075 alloy during electrochemical step under employed operation conditions.

The surface wettability of the HT-Ce and HT-Ce-S layers has been assessed by water contact angle (CA) measurements. Figure 6 comparatively shows the determined water CAs of the bare 7075 alloy after surface preparation treatment and the two investigated conversion coatings, both initially and after continuous immersion in 0.5 M NaCl solution for 360 h. As illustrated in Figure 6, the bare 7075 alloys exhibited hydrophilic characteristics, with CA values around 31°. The presence of HT conversion layer decreased the CA up to ≈11° (not shown here), probably due to the presence of the hydrophilic mixed oxy-hydroxide.

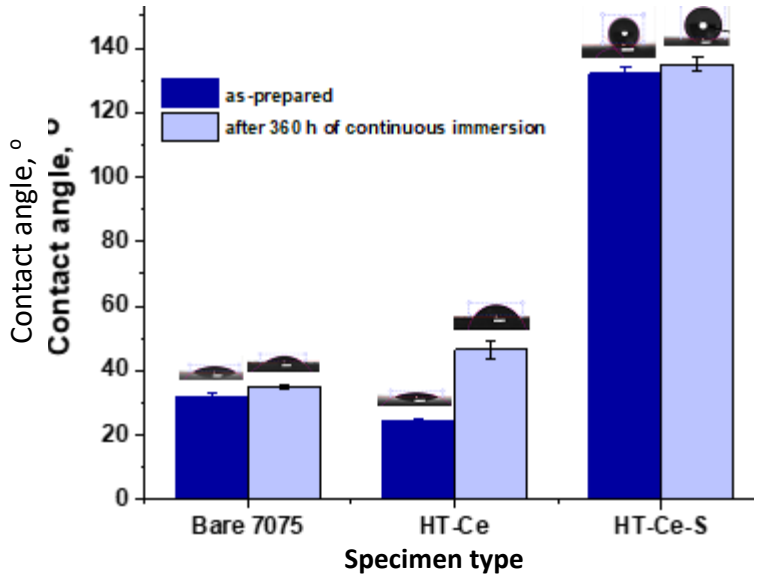

***Figure 6**. Contact angles of bare 7075 alloy after surface pretreatment, of HT-Ce and HT-Ce-S coatings: as-prepared (dark blue) and after 360 h of continuous immersion in 0.5 M NaCl (light blue)*

The chemical cerium insertion to produce HT-Ce coatings does not produce a significant CA modification, the developed surface showing CA values of ≈24.5°, as the porous structure of pristine HT is dominant. On the contrary, the use of the electrodeposition step at constant voltage significantly modified the water CA, whose values are about 132°, suggesting hydrophobic characteristics. Consequently, the resulted surface shows water repellency, leading to a potential enhancement of corrosion performance. After the continuous immersion test, the conversion coatings retained their initial characteristics, *i.e.* HT-Ce-S layers retained their hydrophobicity and HT-Ce remained hydrophilic.

To evaluate the corrosion performance of the developed cerium containing conversion coatings, potentiodynamic polarization curves and electrochemical impedance spectra at open circuit

potential in a free-aerated 0.5 M NaCl solution at room temperature have been recorded after various immersion periods. Typical polarization plots in semilogarithmic coordinates corresponding to HT-Ce and HT-Ce-S conversion layers are presented in Figure 7. For comparison, the same experiments have been carried out for untreated 7075 alloy.

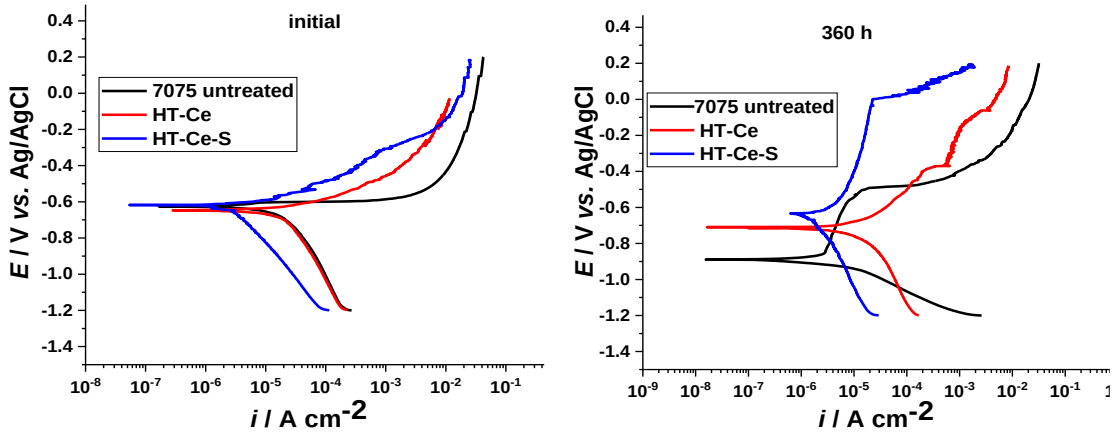

Figure 7. *Polarization curves in semilogarithmic coordinates of bare 7075 alloy, HT-Ce and HT-Ce-S conversion layers in 0.5 M NaCl for the initial and final moments of the continuous immersion test (25 °C, 1 mV s^{-1})*

As shown in Figure 7, the curves recorded at the initial moment of immersion for HT-Ce and HT-Ce-S conversion layers display a slight shift of the corrosion potential towards the electropositive direction, with about 60 and 80 mV, respectively, as compared to untreated alloy. No passive film was formed on a bare 7075 alloy electrode and metal dissolution could be noticed by the shape of the anodic branch of the polarization curve.

A shift of the cathodic branch of the polarization curve to lower current densities could be noticed in the case of cerium-based conversion layers, more significant in the case of the hydrophobic HT-Ce-S layer. This is due to the cathodic inhibition that cerium species may provide.

As the Ce content in HT-Ce-S film was found to be usually higher as compared to the values detected in HT-Ce one, this behavior is much more pronounced in the case of HT-Ce-S coating. The Tafel curves after 360 h of conditioning showed lower currents compared to the initial moment as a result of the protective action of Ce species in the case of the HT-Ce layer and also associated with its hydrophobic nature in the case of HT-Ce-S one. Moreover, as the layers exhibit certain porosity, as SEM micrographs presented earlier evidenced, the additional formation of an aluminum mixed oxide/hydroxide passive film could be possible, which is a usual phenomenon in the case of immersion in aerated solutions. This adds supplementary protection, as well.

Table 3. *Values of corrosion parameters determined from polarization curves for bare 7075, HT-Ce and HT-Ce-S conversion coatings immersed in 0.5 M NaCl*

Substrate type	Initial		After 360 h	
	E_{corr} / V *vs.* Ag/AgCl	j_{corr} / µA cm^{-2}	E_{corr} / V *vs.* Ag/AgCl	j_{corr} / µA cm^{-2}
7075 untreated	-0.601	11.6	-0.757	15.6
HT-Ce	-0.654	8.52	-0.716	5.23
HT-Ce-S	-0.634	2.01	-0.644	1.45

The corrosion current density, j_{corr}, and corrosion potential, E_{corr}, were determined by Tafel extrapolation of both linear portions of cathodic and anodic polarization curves and their values for the investigated specimens are summarized in Table 3.

As shown in Table 3, Ce-based conversion layers significantly improve the aluminum alloy's corrosion performance. Thus, on the initial moment of immersion, values of corrosion current of about 11 µA cm^{-2} for bare alloy have been determined, which decreased up to ≈8.5 µA cm^{-2} and to ≈2 µA cm^{-2} for HT-Ce and HT-Ce-S, respectively. After 360 h of exposure, lower corrosion currents were evidenced in the case of Ce-based conversion coatings, also associated with a positive shift of the corrosion potential. The increase of the j_{corr} in the case of the bare alloy is evidenced as a result of the continuation of the metal dissolution process. In addition, the lowest j_{corr} could be observed in the case of the hydrophobic HT-Ce-S layer, which could be attributed to the synergic action of the presence of cerium species and of the hydrophobic nature of the coating, also associated with the presence of an aluminum mixed oxide/hydroxide passive film.

The electrochemical impedance spectra of HT-Ce and HT-Ce-S conversion layers recorded at open circuit potential (OCP) in 0.5 M NaCl solution for various immersion periods are presented in Figs 8 and 9 as Nyquist and Bode plots. The proposed electrical equivalent circuits (EECs) to describe the corrosion behavior of HT-Ce and HT-Ce-S conversion films are shown in Figure 10.

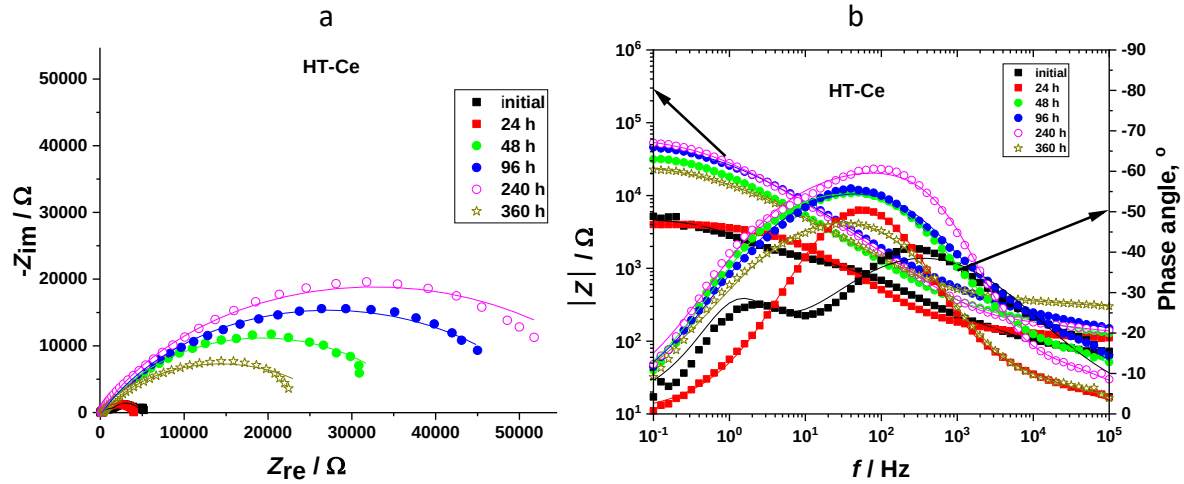

***Figure 8**. Nyquist (a) and Bode (b) plots for HT-Ce conversion coating in 0.5 M NaCl at open circuit potential after various continuous immersion periods (solid lines are the fit to the measured points using the electrical equivalent circuits shown in Figure 10; S_{WE} = 0.196 cm^2)*

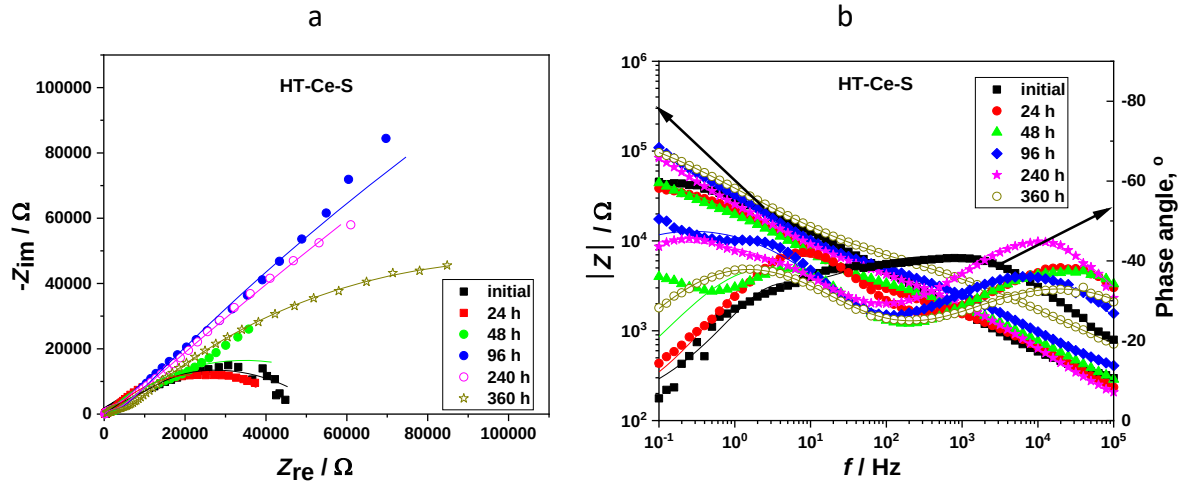

***Figure 9**. Nyquist (a) and Bode (b) plots for HT-Ce-S conversion coating in 0.5 M NaCl at open circuit potential after various continuous immersion periods (solid lines are the fit to the measured points using the equivalent circuit shown in Figure 10; S_{WE} = 0.196 cm^2)*

All Nyquist diagrams show a semicircle arc in the relative high-frequency range. The diameter of the semicircles is usually related to the film resistance and may be correlated to the rate of corrosion: the larger the resistance, the lower the rate of corrosion.

In the case of HT-Ce conversion layers, two times constants are evidenced in the Bode plot (see Figure 8) from the initial moment of immersion up to the end of exposure, attributed to the porous HT layer possibly filled with cerium ionic species as well as to the corrosion process at the metallic substrate/HT interface [48,49,52].

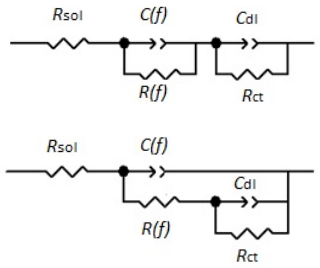

AA7075 / HT-Ce-S; 24, 48, 96, 240 and 360 h of immersion

AA7075 / HT-Ce, initial moment of immersion
AA7075 / HT-Ce, 24, 48, 96, 240 and 360 h of immersion
AA7075 / HT-Ce-S, initial moment of immersion

Figure 10*. The electrical equivalent circuits used to fit the impedance spectra (Figs. 8 and 9) recorded during 360 h of immersion in 0.5 M NaCl solution. The significance of circuit components:* R_{sol}*-ohmic resistance of solution;* C_{dl}*-double layer capacitance;* R_{ct}*-charge transfer resistance;* C*(f) and* R*(f) – capacitance and ohmic resistance of the formed film*

For the HT-Ce-S coated specimens, two time constants are noticed in the Bode plot from Figure 9. The time constant located in the high-frequency region could be related to the electrodeposited cerium stearate, while the second one from the lower frequency could be attributed to the porous HT layer.

The values of the phase angle at the high frequency increase up to 240 h of exposure being also associated with higher impedance modulus, as an indicator of the barrier properties of the electrodeposited layer. This could be attributed to the deposition of cerium oxide/hydroxide at the external part of the HT porous structure, suggesting possible active corrosion protection. Furthermore, up to 360 h of immersion, the phase angle value decreased both at the high-frequency and at the lower-frequency regions due to the damage of the electrodeposited layer containing cerium oxide/hydroxide and possibly due to the corrosion process as a result of the possible infiltration of water and chloride ions through the pores.

In order to fit the experimental electrochemical impedance data and get more quantitative information on the corrosion performance of the investigated Ce-based conversion layers, several electrical equivalent circuits have been tested and those showing the lowest chi-squared (*i.e.* χ^2 in the range $3\times10^{-4} \div 6\times10^{-3}$) and minimum error have been selected, as it was previously detailed in Figure 10. During the fitting of the experimental data we used constant phase elements (CPEs) instead of capacitances [28,48,53] in order to model more accurately the nonideal capacitive behavior of the electrode/electrolyte interface. Rsol represents the ohmic resistance of the solution. *C*(*f*) and *R*(*f*) represent the capacitance and resistance of the formed conversion layer, which might be filled by cerium species, while C_{dl} and R_{ct} stand for the double layer capacitance and charge transfer resistance at metal substrate.

The evolution of *R*(*f*) and *R*ct against the immersion period for HT-Ce and HT-Ce-S layers is shown in Figure 11(a) and Figure 11(b). *R*(*f*) shows a quite similar trend for both investigated conversion coatings. However, it should be noticed that *R*(*f*) values of HT-Ce-S layers are about one order of magnitude higher than HT-Ce ones.

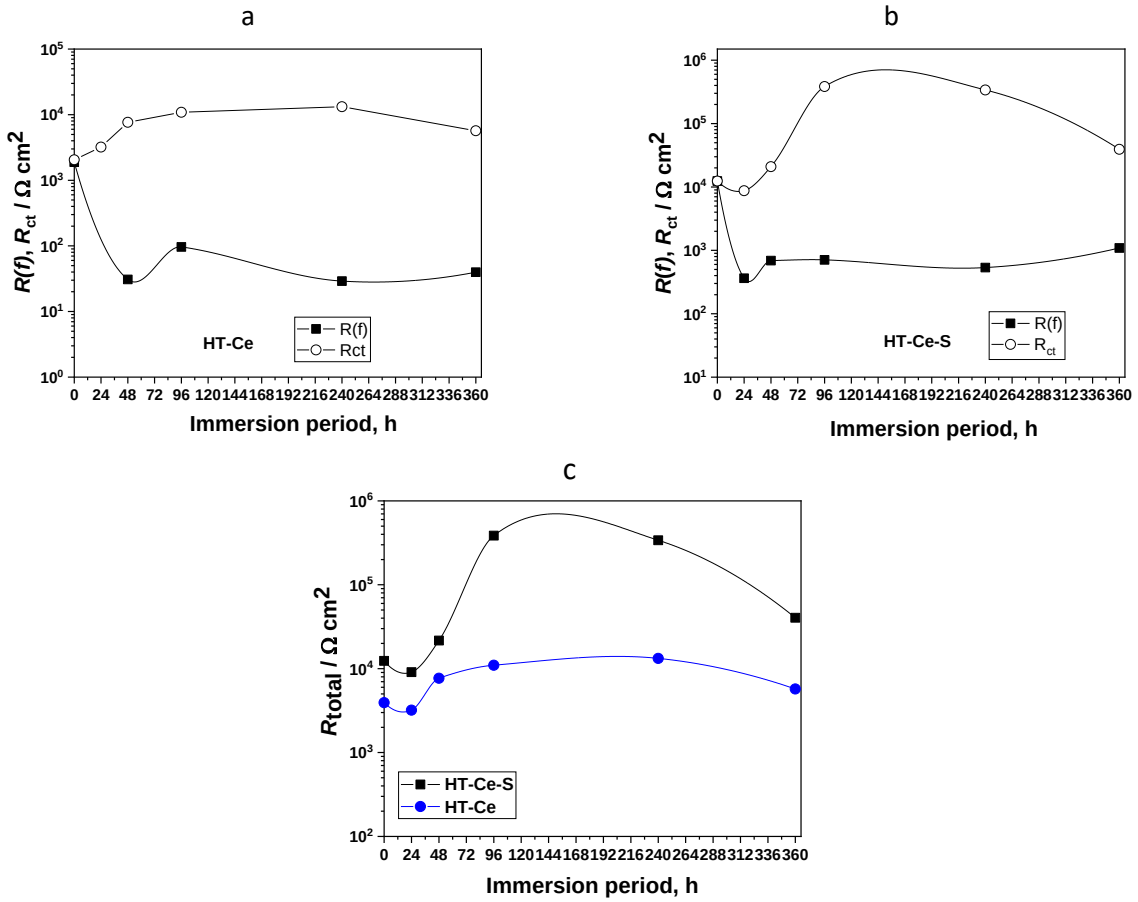

***Figure 11**. Evolution of:* R(f) *and* R_{ct} *for HT-Ce (a) and HT-Ce-S (b) as well as of* R_{total} *(c) for the Ce-based conversion layers against immersion duration in 0.5 M NaCl*

Correspondingly, R_{ct} values of HT-Ce-S layers are larger than those of HT-Ce ones. The R_{ct} values of HT-Ce coated alloy increased gradually up to 96 h, then remained almost constant up to 240 h, suggesting certain corrosion protection during immersion. After 360 h of exposure, a slight decrease of R_{ct} occurs, suggesting the ingress of chloride ions and damaging the integrity of the layer. The R_{ct} values of HT-Ce-S coated alloy are significantly larger as compared to HT-Ce ones and increase faster. This could be attributed to the synergic effect of the higher content of cerium species which may enhance the active corrosion protection and of the non-wetting characteristics of the layer. Indeed, on removing the specimens from the aggressive solution, the visual examination of HT-Ce-S coated alloy specimens showed no surface modifications, while HT-Ce coated alloy samples evidenced a number of corrosion spots.

As different electrochemical parameters have been used to analyze the processes occurring at the conversion layer/metal interfaces, the total resistance R_{total} was determined and its evolution against the immersion time is illustrated in Figure 11c. R_{total} includes the resistance of the conversion layer and the charge transfer resistance, *i.e.,* $R_{total} = R(f) + R_{ct}$ and could represent a useful tool to assess the corrosion performance. As shown in Figure 11c, the HT-Ce-S conversion layers provide the best corrosion protection, evidenced by R_{total} values of about two orders of magnitude higher than HT-Ce ones.

In addition, it can be noticed that R_{total} progressively increased to 96 h and kept the relatively high values up to 240 h, indicating possible active corrosion protection provided by the cerium species as stearate. Moreover, the occurrence of the hydrophobic characteristics prevents the chloride ions ingress.

Conclusions

As a result of the performed investigations, several procedures applied to incorporate Ce species in hydrotalcite–type chemical conversion coatings have been proposed and applied on AA 7075 aluminum alloy and their impact on the overall corrosion performance has been assessed.

The chemical route involving immersion in cerium nitrate solutions produced a porous morphology, entirely covering the metallic surface, exhibiting hydrophilic characteristics. The EDX analysis evidenced a content of 2.46 – 6.84 wt.% Ce in the composition of HT-Ce layer.

The electrochemical process involving ethanolic solutions of stearic acid and cerium nitrate and an applied constant voltage led to the formation of a hydrophobic cerium stearate conversion layer on aporous HT conversion coating. A better profiled curved platelet structure developed perpendicular to the substrate was evidenced, also exhibiting a certain level of disorder. Based on EDX measurements, the Ce content within the HT-Ce-S layer was found to be higher, in the range 6.55 - 9.73 wt.%. The calculated C/Ce atomic ratio was between 49.5 and 52.77, very close to the theoretical value in cerium stearate. The electrochemically produced HT-Ce-S layers exhibited hydrophobic characteristics, materialized by water contact angles of about 132°.

Based on preliminary experimental results, the electrochemically prepared HT-Ce-S conversion layers onto AA7075 alloy showed improved corrosion performance compared to chemically produced HT-Ce ones, materialized in corrosion current densities of 1-2 μA cm^{-2} and total resistances of 340-385 kΩ cm^2. This behavior could be attributed to the synergic effect of the higher content of cerium species which may enhance the active corrosion protection and the hydrophobic characteristics of the conversion layer.

Finally, future investigations are scheduled for better optimization of the electrochemical conversion process to achieve a better long-term corrosion performance and to design an industrially compliant technological process.

Acknowledgements: *The financial support for this work was under the ECOCCEALPROT project 311PED/2020.*

References

[1] W. Nickerson, C. Matzdorf, *Non-Chromate Aluminum Pre-treatments – Final Report*, Project WP-200025/2012. https://apps.dtic.mil/sti/pdfs/ADA582070.pdf (accessed February 2022)

[2] A. M. Pereira, G. Pimenta, B. D. Dunn, *Assessment of Chemical Conversion Coatings for the Protection of Aluminium Alloys - A Comparison of Alodine 1200 with Chromium-Free Conversion Coatings*, ESA STM-276 /2008, European Space Agency; http://esmat.esa.int/ESA-STM-276.pdf (accessed February 2022)

[3] A. D. Nicolo, L. Paussa, A. Gobessi, A. Lanzutti, C. Cepek, F. Andreatta, L. Fedrizzi, *Surface and Coatings Technology* **287** (2016) 33-43. http://doi.org/10.1016/j.surfcoat.2015.12.059

[4] N. C. Rosero-Navarro, M. Curioni, Y. Castro, M. Aparicio, G. E. Thompson, A. Durán, *Surface and Coatings Technology* **206** (2011) 257-264. http://doi.org/10.1016/j.surfcoat.2011.07.006

[5] A. E. Hughes, T.G. Harvey, N. Birbilis, A. Kumar, R. G. Buchheit, *Coatings for corrosion prevention based on rare earths,* in *Rare Earth-Based Corrosion Inhibitors,* M. Forsyth, B. Hinton (Eds.), Woodhead Publishing Series in Metals and Surface Engineering No. 61, Elsevier, 2014, p. 186-232.

[6] G. Bierwagen, R. Brown, D. Battocchi, S. Hayes, *Progress in Organic Coatings* **68** (2010) 48-61. https://doi.org/10.1016/j.porgcoat.2009.10.031

[7] O. Gharbi, S.Thomas, C. Smith, N. Birbilis, *npj Materials Degradation* **2** (2018) 12. https://doi.org/10.1038/s41529-018-0034-5
[8] R. G. Buchheit, S. B. Mamidipally, P. Schmutz, H. Guan, *Active corrosion protection in chromate and chromate free conversion coatings*. Scientific Report Ohio State University, 2000. https://www.academia.edu/23404374/Active_Corrosion_Protection_in_Chromate_and_Chromate_Free_Conversion_Coatings
[9] M. W. Kendig, R. G. Buchheit, *Corrosion* **59(5)** (2003) 379-400. https://doi.org/10.5006/1.3277570
[10] G. Harvey, *Corrosion Engineering, Science and Technology* **48(4)** (2013) 248-269. https://doi.org/10.1179/1743278213Y.0000000089
[11] M. F. Montemor, *Fostering Green Inhibitors for Corrosion Prevention*, in *Active Protective Coatings. New-Generation Coatings for Metals*, A. E. Hughes, J. M. C. Mol, M. L. Zheludkevich, R. G. Buchheit (Eds.), Springer Series in Materials Science vol. 233, Springer Science+Business Media, Dordrecht, Holland, 2016, p. 107
[12] J. J. Alba-Galvín, L. González-Rovira, M. Bethencourt, F. J. Botana, J. M. Sánchez-Amaya, *Metals* **9** (2019) 320. https://doi.org/10.3390/met9030320
[13] P. Campestrini, H. Terryn, A. Hovestad, J. H. W. de Wit, *Surface and Coatings Technology* **176** (2004) 365-381. https://doi.org/10.1016/S0257-8972(03)00743-6
[14] B. W. R. Hinton, D. R. Arnott, N. E. Ryan, *Metals Forum* **4** (1984) 211-217. https://www.researchgate.net/publication/280014915_inhibition_of_aluminum_alloy_corrosion_by_cerous_cations
[15] B. W. R. Hinton, D. R. Arnott, N. E. Ryan, *Materials Forum* **9(3)** (1986) 162-173. https://www.researchgate.net/publication/279891652_Cerium_Conversion_Coatings_for_the_Corrosion_Protection_of_Aluminum
[16] A. E. Hughes, J. D. Gorman, P. J. K. Paterson, *Corrosion Science* **38** (1996) 1957-1976. https://doi.org/10.1016/S0010-938X(96)00088-1
[17] A. de Frutos, M. A. Arenas, Y. Liu, P. Skeldon, G. E. Thompson, J. de Damborenea, A. Conde, *Surface and Coatings Technology* **202** (2008) 3797-3807. https://doi.org/10.1016/j.surfcoat.2008.01.027
[18] S. G. Hardin, K. W. Wittel, A. E. Hughes, K. J. H. Nelson: Process and solution for providing a conversion coating on a metallic surface, World Intellectual Property Organization Patent WO-2001-071059, 2001.
[19] A. I. Khan, D. O'Hare, *Journal of Materials Chemistry* **12** (2002) 3191-3198. https://doi.org/10.1039/B204076J
[20] T. N. Shulha, M. Serdechnova, S. V. Lamaka, D. C. F. Wieland, K. N. Lapko, M. L. Zheludkevich, *Scientific Reports* **8** (2018) 16409. https://doi.org/10.1038/s41598-018-34751-7
[21] R. G. Buchheit, P. G. Schmutz, H. G. Guan, S. B. Mamidipally, *Corrosion* **58** (2002) 3-14. https://doi.org/10.5006/1.3277303
[22] P. Visser, Y. Liu, X. Zhou , T. Hashimoto , G.E. Thompson, S.B. Lyon, L.G.J. van der Ven, A.J.M.C. Mol, H. A. Terryn, The corrosion protection of AA2024-T3 aluminium alloy by leaching of lithium-containing salts from organic coatings, *Faraday Discussions* **180** (2015) 511-526. https://doi.org/10.1039/C4FD00237G
[23] P. Visser, Y. Gonzalez-Garcia, J. M. C. Mol, H. Terryn, *Journal of the Electrochemical Society* **165** (2018) C60-C70. https://doi.org/10.1149/2.1011802jes
[24] R. G. Buchheit, M. D. Bode, G. E. Stoner, *Corrosion* **50(3)** (1994) 205-214. https://doi.org/10.5006/1.3293512
[25] C. A. Drewien, M. O. Eatough, D. R. Tallant, C. R. Hills, R. G. Buchheit, *Journal of Materials Research* **11** (1996) 1507-1513. https://doi.org/10.1557/JMR.1996.0188

[26] P. Visser, H. Terryn, J. M. C. Mol, *Surface and Interface Analysis* **51** (2019) 1276-1287. https://doi.org/10.1002/sia.6638
[27] S. M. C. Fernandes, O. V. Correa, J. A. Souza, R. A. Antunes, N. B de Lima, L. V. Ramanathan, *Preparation and characterization of hydrotalcite coatings to protect aluminum alloys*, 22º CBECiMat - Congresso Brasileiro de Engenharia e Ciência dos Materiais, 6-10 November 2016, Natal, RN, Brasil, p. 6793-6804
[28] Y. Zhang, J. Liu, Y. Li, M. Yu, X. Yin, S. Li, *Journal of Wuhan University of Technology, Materials Science Edition* **32** (2017) 1199-1204. https://doi.org/10.1007/s11595-017-1731-6
[29] Y. Zhang, Y. Li, Y. Ren, H. Wang, F. Chen, *Materials Letters* **192** (2017) 33-35. https://doi.org/10.1016/j.matlet.2017.01.038
[30] M. A. Iqbal, M. Fedel, *Advances in Materials Science and Engineering* **2020** (2020) 5785393. https://doi.org/10.1155/2020/5785393
[31] M. Fedel, M. Zampiccoli, *Applied Sciences* **11** (2021) 8252. https://doi.org/10.3390/app11178252
[32] Y. Cao, D. Zheng, F. Zhang, J. Pan, C. Lin, *Journal of Materials Science & Technology* **102** (2022) 232-263. https://doi.org/10.1016/j.jmst.2021.05.078
[33] B. Yang, Y. Ma, Z. Liang, Y. Liao, Z. Wang, P. Zhu, *Surface and Coatings Technology* **405** (2021) 126629. https://doi.org/10.1016/j.surfcoat.2020.126629
[34] M. A. Iqbal, H. Asghar, M. Fedel, *Journal of Alloys and Compounds* **844** (2020) 156112. https://doi.org/10.1016/j.jallcom.2020.156112
[35] G. Boisier, A. Lamure, N. Pébère, M. Villatte, *Surface and Coatings Technology* **203** (22) (2009) 3420-3426. https://doi.org/10.1016/j.surfcoat.2009.05.008
[36] M. A. Iqbal, H. Asghar, M. Fedel, *Solids* **2** (2021) 76-86. https://doi.org/10.3390/solids2010004
[37] B. Zhang, Y. Li, B. Hou, *RSC Advances* **5** (2015) 100000-100010. https://doi.org/10.1039/C5RA21525K
[38] B. Zhang, Q. Zhu, Y. Li, B. Hou, *Chemical Engineering Journal* **352** (2018) 625-633. https://doi.org/10.1016/j.cej.2018.07.074
[39] V. Gordovskaya, M. Curioni, T. Hashimoto, J. Walton, G. E. Thompson, P. Skeldon, *Journal of the Electrochemical Society* **163(6)** (2016) C253-C259. https://doi.org/10.1149/2.0201606jes
[40] L. Anicai , A. C. Manea, T. Visan, *Molecular Crystals and Liquid Crystals* **418(1)** (2004) 41-53. https://doi.org/10.1080/15421400490478948
[41] R. Andreeva, E. Stoyanova, A. Tsanev, M. Datcheva, D. Stoychev, *International Journal of Electrochemical Science* **13** (2018) 5333-5351. https://doi.org/10.20964/2018.06.71
[42] C. M. Rangel, T. I. Paiva, P. P da Luz, *Surface and Coatings Technology* **202** (2008) 3396-3402. https://doi.org/10.1016/j.surfcoat.2007.12.017
[43] C. M. Rangel, T. I. Paiva, *Portugaliae Electrochimica Acta* **18** (2000) 13-21. https://doi.org/10.4152/pea.200001013
[44] M. Datta, D. Landolt, *Electrochimica Acta* **45(15-16)** (2000) 2535-2558. Https://doi.org/10.1016/S0013-4686(00)00350-9
[45] P. Villars, K. Cenzual, Pearson's Crystal Data: Crystal Structure Database for Inorganic compounds (on CD-ROM), Version 1.0, Release 2007/8, ASM International, Materials Park, Ohio, USA, Entry 251015
[46] W. Wu, F. Zhang, Y.-C. Li, Y.-F. Zhou, Q.-S. Yao, L. Song, R.-C. Zeng, S. C. Tjong, D.-C. Chen, *Frontiers of Materials Science* **13(4)** (2019) 420-430. https://doi.org/10.1007/s11706-019-0476-x

[47] R. Allmann, H. P. Jepsen, *Neues Jahrbuch fur Mineralogie, Monatshefte* **1969** (1969) 544-551.
[48] K. Lin, X. Luo, X. Pan, C. Zhang, Y. Liu, *Applied Surface Science* **463** (2019) 1085-1096. https://doi.org/10.1016/j.apsusc.2018.09.034
[49] C. Zhang, X. Luo, X. Pan, L. Liao, X. Wu, Y. Liu, *Applied Surface Science* **394** (2017) 275-281. https://doi.org/10.1016/j.apsusc.2016.10.034
[50] H. Wang, G. Fan, C. Zheng, X. Xiang, F. Li, *Industrial & Engineering Chemical Research*, **49** (2010) 2759-2767. https://doi.org/10.1021/ie901519h
[51] F. Di Franco, A. Zaffora, P. Vassallo, M. Santamaria, *Journal of the Electrochemical Society* **168** (2021) 101502. https://doi.org/10.1149/1945-7111/ac29df
[52] M. A. Iqbal, L. Sun, A. T. Barrett, M. Fedel, *Coatings* **10** (2020) 428. https://doi.org/10.3390/coatings10040428
[53] S. Abirami, T. Bharathidasan, S. Sathiyanarayanan, *Corrosion* **77(10)** (2021) 1080-1099. https://doi.org/10.5006/3799